Chapter 6

Evolving manifolds, by K.FRISCHMUTH

Selected topics in Geometry and Mathematical Physics,
Vol. 1, 2002, pp. 161-187.

Numerical methods for evolving manifolds and applications in rail-wheel contact mechanics[1]

Abstract In this paper[2] we study processes related to evolving manifolds the motion of which is governed by a speed law for the normal velocity in terms of a description of the actual shape of the surface. Well-known special cases of this

[1]**Kurt Frischmuth**, FB Mathematik, Universität Rostock, D-18051 Rostock, www: http://alf.math.uni-rostock.de/~kurt/Welcome.html , e-mail: kurtsun2.math.uni-rostock.de

[2]This paper was encouraged by il mio caro amico Vito Antonio Cimmelli whom I visited in October 2000 in Universitá della Basilicata, Potenza, Italy. During my stay in Potenza I held a series of lectures the content of which is summarized in this publication.

general problem are curvature driven flows. We study numerical approaches to the simulation of such processes. The results are applied to a problem in railway mechanics. The change of profile geometry due to wear is considered as evolution problem. The speed law for a single wheelset is derived from an analysis of forces acting on a rigid wheel and the resulting motion. ——— Italy. ———

6.1 Introduction

The aim of this paper is to embed recent results in the study of wear phenomena in railway mechanics into the framework of the theory of evolving manifolds.

In the first part of this paper we study *academic evolution problems*, i.e., we assume a *speed law* is given and expressed by an analytic formula. We study two approaches to a numerical solution. The first one is straightforward, based on a parameterization of the manifold under investigation. We assign a number of *markers* to fixed parameter values, and then study the trajectories of those markers. This is comparable with a Lagrangean approach to continuum mechanics where we have particles instead of markers. The difference is that the markers in general are artificial and arbitrary, they do not correspond to anything physical. As a consequence, marker trajectories may intersect, or at least the distribution of markers can become problematic.

As an alternative we present the *level set* approach, which is based on an implicit representation of the manifold in the form $\Phi(x,t) = 0$. Here we move the graph of the function Φ up or down in order to achieve the desired motion of the zero level set in the space of x-coordinates. It turns out that – if properly implemented – this method has considerable advantages.

In the second part we study rail–wheel contact problems. Here the speed law is determined by factors responsible for wear. In order to evaluate the normal speed of wear at the surface of a wheel we have to simulate the motion of the railway vehicle the wheel is part of, calculate *contact forces* and *relative speeds* of the bodies in contact, and eventually determine the *frictional power dissipation*. Assuming that wear is abrasive only, following a classical hypothesis wear speed is proportional to frictional power, the speed law is thus defined up to a factor. Hence, obviously, the calculation of the speed

law is numerically very expensive in this *non-academic case* of a surface evolution problem. To keep things as simple as possible we study as example of a vehicle just a rigid wheelset pulled at prescribed speed along a straight ideal track.

Note that evolution of a wear surface happens in a time scale of several hundreds of thousands of turns of a wheel. The motion of a wheelset is highly repetitive. Even if not periodic, a temporal mean value of power dissipation is usually approached after just a couple of turns. It depends on the actual wheel geometry, but it is independent from initial conditions imposed on the multibody system coordinates of the vehicle. Thanks to this property (ergodicity) we do not need to calculate complete trajectories of a vehicle for the lifetime of the part we are interested in. Instead, we identify the actual normal speed on the surface (as a whole) by simulating just a short piece of trajectory typical of the present wheel geometry. Timestepping is done by the same algorithm as in the academic case. Not surprisingly, naive methods may lead to artificial oscillations of the wear patterns obtained. We study this effect under the assumption of round wheels, for out-of-the-round wheels we refer to [11, 12, 13, 19].

6.2 Evolving manifolds

6.2.1 Evolution equation

Let a manifold $\mathcal{M}_t \subset \mathbf{R}^n$ be given by

$$x = x(t, \tau) \tag{6.1}$$

where t denotes time, $\tau \in \mathcal{T}$ an element of the parameter space $\mathbf{R}^d$ and $x \in \mathbf{R}^n$ is a position in physical space on the actual surface we are studying. In our main application, we have $n = 3$ and $d = 2$. For examples we often reduce dimensions by one, thus we have curves instead of surfaces. In the sequel we will restrict ourselves to the presentation of the two-dimensional case.

Note that later, in the second part of this paper, the surface

$$\mathcal{M}_t = \{x(t, \tau) \,|\, \tau \in \mathcal{T}\} \tag{6.2}$$

plays the role of the reference configuration of the wheel surface, which is subject to rolling motion and contact with rails. For this second part, $\mathcal{M}_t$ is frozen, and time – again denoted by t – runs as a local variable. Restriction to the 2d case can be considered either as a study of the profile or of the circumference. Here we concentrate on the profile evolution.

We introduce tangential and normal vectors to $\mathcal{M}_t$

$$\vec{t} = \frac{x'}{g} = x_\tau(t,\tau)g^{-1} \quad \text{with} \quad g = \|x'\| = \sqrt{x' \cdot x'} \tag{6.3}$$

$$\vec{n} = Q\,\vec{t} \quad \text{with} \quad Q = \begin{pmatrix} 0 & 1 \\ -1 & 0 \end{pmatrix} \tag{6.4}$$

The fundamental equation of manifold evolution is now

$$\dot{x} = x_t(t,\tau) = \mathcal{F}\vec{n} \quad . \tag{6.5}$$

For convenience we denote time-derivatives by a superposed dot and derivatives with respect to τ by a prime. Moving along with the curve at fixed parameter value τ, we observe a change in tangential direction due to varying speed along the curve. Furthermore, the curve may stretch and change curvature.

Simple academic examples of evolution problems arise if we assume a constant speed function $\mathcal{F}$, e.g. $\mathcal{F} = +1$ or $\mathcal{F} = -1$. For a sphere (or a circle in 2d) we can solve the problem analytically, obtaining an expansion, respectively implosion, the latter restricted to a time interval equal to the initial radius of the sphere. We anticipate trouble for evolution towards the center of curvature around time $t = 1/\kappa_{max}$ where κ_{max} is the maximum of curvature along a curve. In our notation the curvature κ is given by

$$\kappa = -\frac{\vec{t}' \cdot \vec{n}}{g}\,. \tag{6.6}$$

If we require some frame independence, $\vec{t}$ should not enter directly the constitutive equation for the normal speed, and the next natural choice is a speed law of the form

$$\mathcal{F} = \mathcal{F}(\kappa)\,. \tag{6.7}$$

Problems of this type are well-known as *curvature driven flows*.

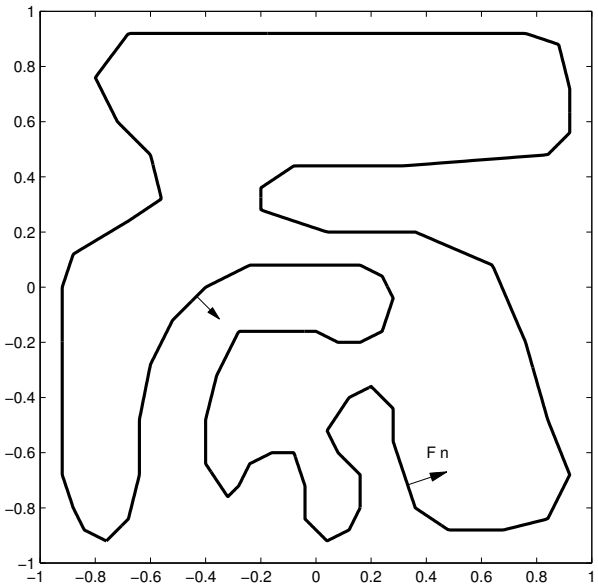

Figure 1: A curve with normal speed at two points.

Using chain-rule we can deduce

$$\dot{g} = \frac{\partial}{\partial t}\sqrt{x'x'} = x'\dot{x}'/g = \vec{t}(F\vec{n})' = \vec{t}FQ(-1)g\kappa\vec{n} = Fg\kappa \quad . \tag{6.8}$$

The change of tangential direction can be obtained from

$$\dot{\vec{t}} = \frac{\partial}{\partial t}\left(\frac{x'}{g}\right) = \frac{\dot{x}'g - x'\dot{g}}{g^2} = \frac{\mathcal{F}_\tau}{g}\vec{n} \quad . \tag{6.9}$$

Hence, given the evolution equation in the form $\mathcal{F} = \mathcal{F}(\kappa)$, we obtain for the time derivative of κ

$$\dot{\kappa} = -\frac{\partial}{\partial t}\left(\frac{\vec{t}'\vec{n}}{g}\right) = -\mathcal{F}\kappa^2 - \frac{1}{g}\left(\mathcal{F}'\kappa'/g\right)' \tag{6.10}$$

As a consequence, for curvature-driven motion, $\mathcal{F} = \mathcal{F}(\kappa)$, given the above formulas for $\dot{g}$ and $\dot{\kappa}$ one easily infers that the sign of the time derivative

of the integral

$$V(t) = \int_{\tau_0}^{\tau_1} |\kappa| g d\tau \tag{6.11}$$

is determined by the sign of $\mathcal{F}'$ at $\kappa = 0$.

In particular, for $\mathcal{F}$ globally decreasing, the total curvature – which can be imagined as elastic energy – diminishes with evolution, i.e., the curve is smoothed. For $\mathcal{F} = -1$, $n = 2$, $d = 1$, Grayson's theorem says that each curve evolves to a convex one which eventually collapses into a point. Rewriting the evolution equation in terms of arc-length as space variable, analogies to Burgers equation can be found. Constant $\mathcal{F}$ corresponds to the hyperbolic case, monotonously decreasing dependence on κ acts as a parabolic regularization. Obviously, in general, evolution breaks down due to the development of corners, see Fig. 3.

6.2.2 Method of markers

A straightforward approach to the solution of the evolution equation is known as the method of markers – which is nothing else than the well-known method of lines in parabolic PDEs. Here one uses a fixed grid in parameter space $\mathcal{T}$. Tangent vector and/or normal vector, if needed also curvature, are calculated from difference approximations for the first, respectively second, derivatives of $x(t, \cdot)$.

Convenient candidates for numerical tests are graphs of functions or closed curves with an analytical representation in both parameter and implicit form, e.g. an ellipse

$$x_1 = a \cos\tau\,, \quad x_2 = b \sin\tau \quad \text{and} \quad \Phi(x) = \frac{x_1^2}{a^2} + \frac{x_2^2}{b^2} - 1 = 0$$

or a Cassini curve

$$x_1 = r(\tau) \sin\tau\,, \quad x_2 = r(\tau) \sin\tau$$

where

$$r(\tau) = \sqrt{c^2 \cos(2\tau) + \sqrt{c^4 \cos^2(2\tau) + a^4 - c^4}}$$

and

$$\Phi(x) = (x^2 + y^2)^2 - 2c^2(x^2 - y^2) - (a^2 - c^2) = 0\,.$$

Later on, however, we will have to deal with surfaces of realistic bodies, given by measurements or industrial standards.

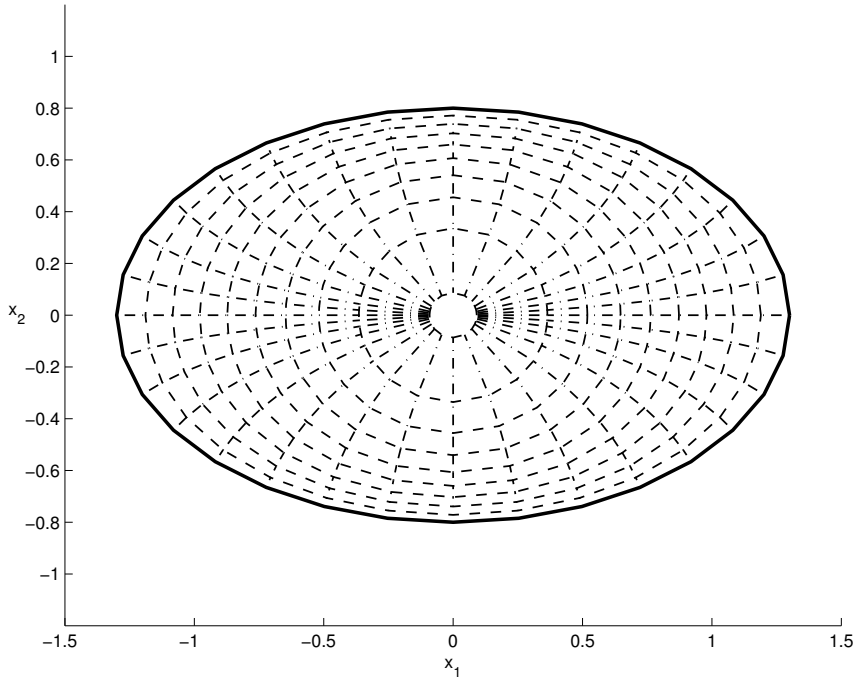

Figure 2: Ellipse collapsing under curvature by tracer method.

Given the relation to hyperbolic and parabolic PDEs it is not surprising that such an approach leads to difficulties. For constant $\mathcal{F}$ one easily finds out that smooth solutions in general do not exist for all $t \geq 0$. Corners may develop at finite time, cf. Fig. 3, as shocks develop in hyperbolic PDEs.

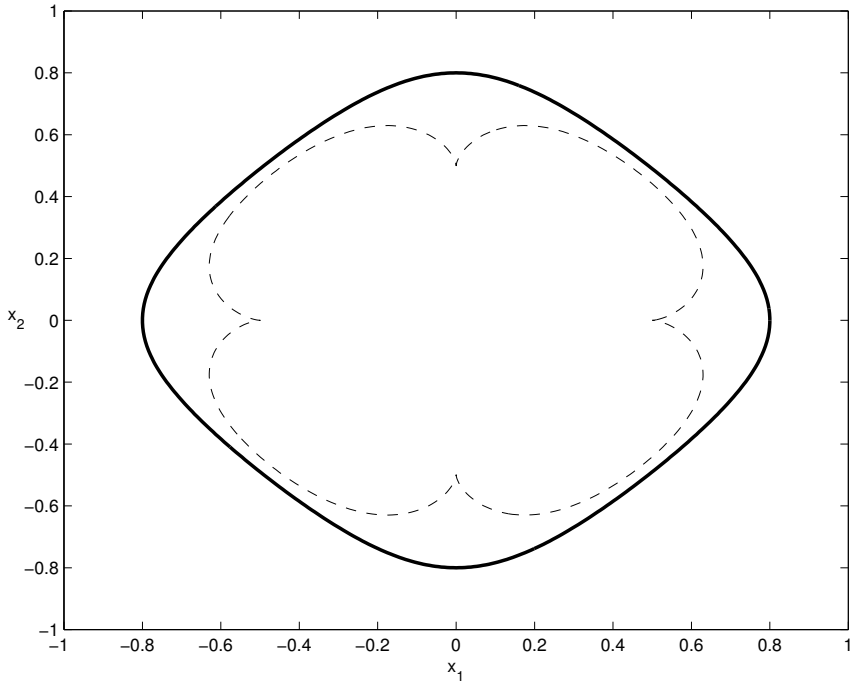

Figure 3: Development of corners.

This is accompanied by a breakdown of symmetric difference formulas. The problem may be solved by a proper choice of one-sided approximations. Further, there is the problem of step size for explicit methods. In analogy to the PDE case, a CFL-condition has to be fulfilled. Given the fact that for fixed distances in $\mathcal{T}$-space the corresponding distances in x-space may shrink with curve evolution (for g decreasing), this implies often extremely short timesteps.

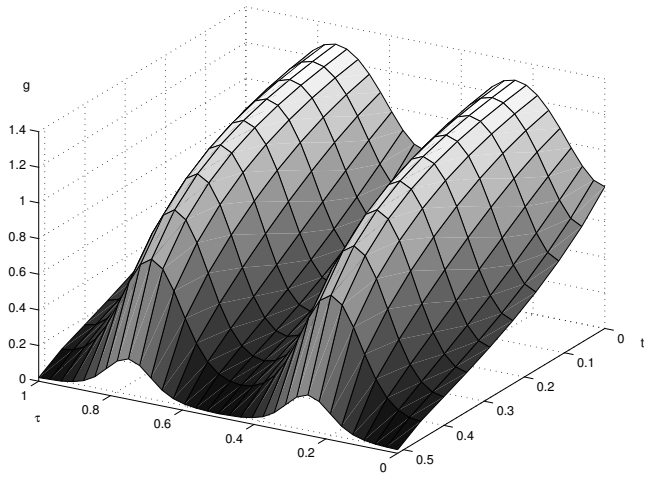

Figure 4: Metric of collapsing ellipse.

While it is possible to implement quite successfully semi-discretizations based on the marker approach by applying appropriate integration methods to the resulting systems of ODEs, results are not too effective. The examples show that markers tend to concentrate in certain regions, while others become very rarified, cf. Fig. 2. This can be overcome by restarting the method regularly with rearranged markers, but we follow a different strategy here.

6.2.3 Level set–formulation

Instead of the representation $x = x(t, \tau)$ and the equations of evolution in the form $v_n(t, \tau) = \dot{x} \cdot \vec{n} = \mathcal{F}$ we switch to defining our curve as zero level set of a function $\Phi(x, t)$ and motion governed by the partial differential equation for Φ

$$\Phi_t(x, t) + \mathcal{F}|\nabla\Phi(x, t)| = 0\,. \tag{6.12}$$

As initial condition we pose

$$\Phi(x, 0) = \Phi_0(x) \quad . \tag{6.13}$$

Note that the choice of Φ_0 is quite arbitrary, $\mathcal{F}$ has to be extended from $\mathcal{M}_0$ to an open neighborhood in $\mathbf{R}^n$. As an example let us study again the

imploding sphere with initial radius $r_0 > 0$. We choose $\Phi_0(x) = |x|^2 - r_0^2 = 0$, $\Phi_t - |\Phi_x| = 0$. The level set function is lifted up, hence the intersection with the zero-plane quickly shrinks to a point and disappears, cf. Fig. 5.

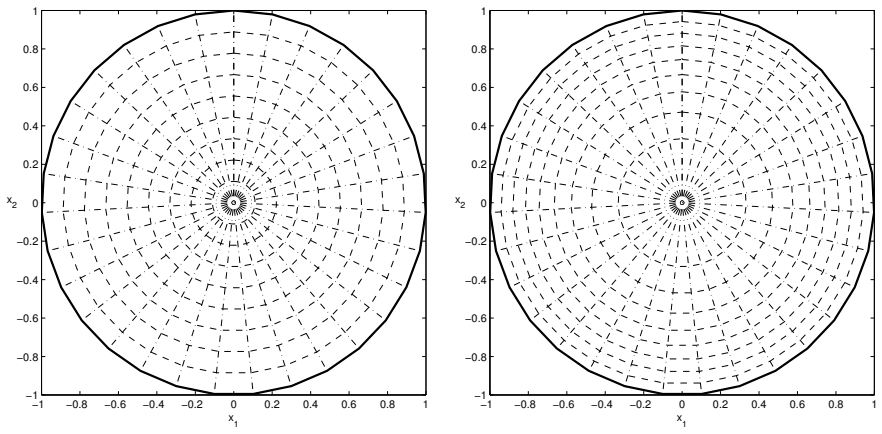

Figure 5: Collapsing spheres with $\mathcal{F} = -1$ and $\mathcal{F} = -\kappa$.

Now, we have to solve a PDE for Φ in a $d+1$-dimensional domain in order to find the evolution of a d-dimensional manifold. While this seems even more ineffective, it can be done very effectively, since high accuracy is only required in a narrow region where values of Φ are close to zero. There is one more significant simplification which is useful in irreversible processes – as in our application of wear surfaces. Removed material can never be reattached, hence for each point of a body undergoing wear it is sufficient to determine when it will be on the surface and rubbed off. This observation leads to the stationary level set method.

Stationary level set approach

In the general case of the level set formulation we look for a function Φ in 1–3 space coordinates and time. Numerical costs can be reduced considerably if it is known a priori that the *front* $\mathcal{M}_t$ passes through each point in space only once.

This is the case e.g. for convex curves and $sgn(\mathcal{F}) \neq 0$.

It is possible to define the motion by determining, for each position x, the instant $T(x)$ when the front passes through x

$$T(x) = \min_{t \in \mathbf{R}} \{x \in \mathcal{M}_t\} \quad .$$

Compatibility with $v_n = \mathcal{F}$ requires now

$$|\nabla T(x)| \mathcal{F} = 1 \, . \tag{6.14}$$

A further simplification can be applied if it is known that the manifold is the graph of a function – in suitable coordinates, e.g. $x_n = \Psi(\bar{x})$, $\bar{x} = (x_1, x_2 \dots x_{n-1})$. Then we set $\Phi(x) = \Psi(\bar{x}) - x_n$, and the whole problem can be solved in terms of $\bar{x} \in \mathbf{R}^{n-1}$. For instance, a non-convex Cassini curve will partially expand before collapsing, hence the stationary approch cannot be applied. Nevertheless the problem can still be treated by solving a one-dimensional PDE instead of a 2D one.

Conservative schemes

The level set approach has the great advantage that the grid does not distort with time, whatever the evolving manifold does. The step sizes, for instance, remain constant. However, naive approximations to $|\nabla \Phi|$ break down as well when it comes to the development of corners.

Successful discretizations are built analogously to such for hyperbolic balance laws of the form $u_t + \varphi(u)_x = 0$. However, here we have $\varphi(u_x)$ instead of $\varphi(u)_x$ with $\varphi(\cdot) \equiv |\cdot|$.

The general idea consists in taking central differences of a *numerical Flux* G instead of numerically differentiating the values of φ themselves. The values of G are assigned to the midpoints between nodes of the x-grid where the u-values are defined

$$G_{i+1/2} = G(u_i, u_{i+1}) \quad . \tag{6.15}$$

The numercal flux in a midpoint depends on both neighboring nodes (or more, the so-called stencil). We require Lipschitz–continuity and consistency with φ in the sense that for constant u we get identical results,

$$G(u, u) = \varphi(u) \quad . \tag{6.16}$$

Obvious variants of the method arise if we substitute for u the one-sided derivatives of Φ (or Ψ) into *well-known* numerical fluxes G – such as Lax–Friedrichs, up-wind or Lax–Wendroff methods. Thus we obtain a general algorithm of the form

$$\Phi_i^{k+1} = \Phi_i^k - \Delta t\, G\left(\frac{\Phi_i^k - \Phi_{i-1}^k}{\Delta x}\,,\ \frac{\Phi_{i+1}^k - \Phi_i^k}{\Delta x}\right) \tag{6.17}$$

Lax–Friedrichs method

$$G(u_1, u_2) = -\frac{\Delta x}{2\Delta t}(u_2 - u_1) + \frac{1}{2}(\varphi(u_2) + \varphi(u_1))$$

upwind method

$$G(u_1, u_2) = \varphi\left(\max(u_1, 0)\right) + \varphi\left(\min(u_2, 0)\right)$$

In Fig. 7 the domain (arbitrarily drawn by mouse) shrinks nicely, staying smooth all the time, without any corners or overlappings. This is due to the regularizing effect of $\mathcal{F} = -\kappa$. Unfortunately, in our main application curvature also plays a role, since it causes accelerations, but the dependence is more complex and the effects are not always smoothing.

The numerical calculation of the manifold evolution reduces to a quite simple recursion. However, there are two additional problems here. First, for start-up a procedure is needed to construct a suitable grid function around the initial contour $\mathcal{M}_0$ that just goes through zero there at a reasonable slope. Finally, as postprocessing it is required to find $\mathcal{M}_t$ as the zero level set of the function Φ while previously a discrete parameterization of $\mathcal{M}_t$ was directly available. Both problems can be solved easily by standard methods, cf. [22].

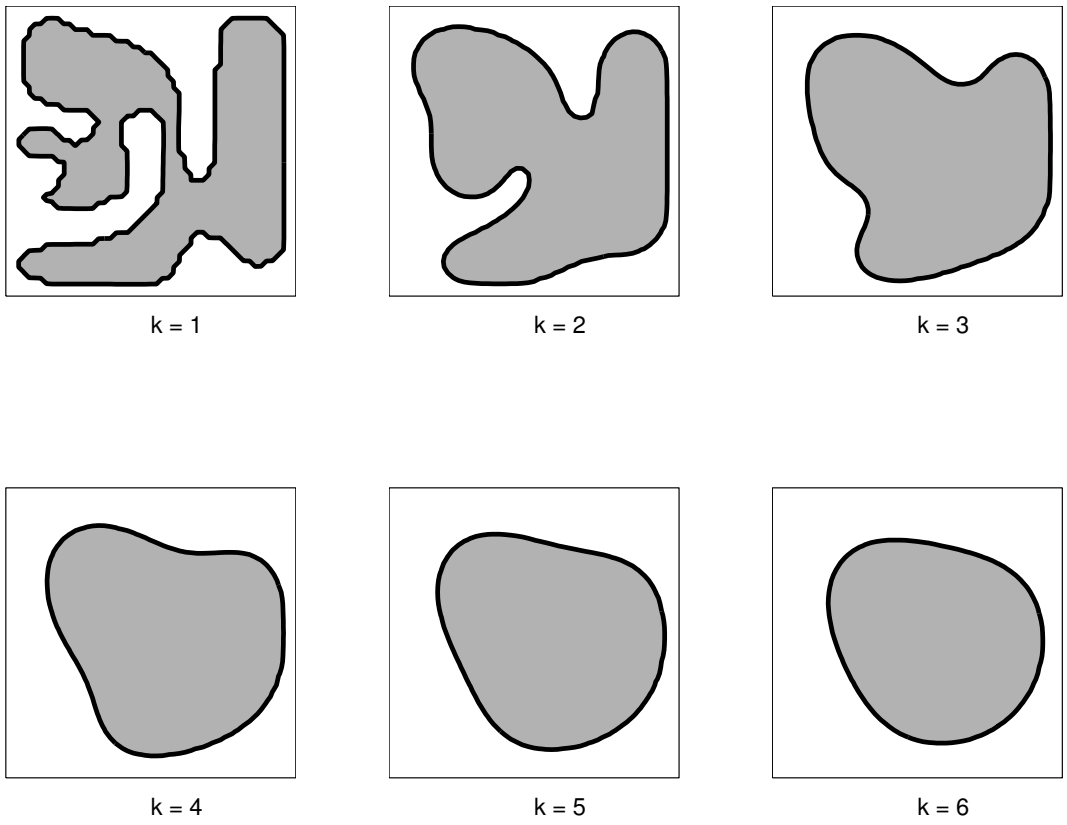

Figure 7: Level set method.

6.3 Rail–Wheel Mechanics

6.3.1 Multibody systems

The present framework of choice for the simulation of vehicles is the theory of multibody systems. Here we outline the basic equations of this approach together with some crucial constituents needed to model a railway vehicle.

In multibody systems positions of all particles under consideration are defined in terms of a finite number of coordinates y (or sometimes $p = p(t)$). Those coordinates may be (preferably) independent, in that case their number – the dimension of y – is referred to as *degrees of freedom*. Otherwise

constraints may be imposed, e.g. in the case of so-called *kinematically closed loops*. In the independent case the temporal changes of y are governed by ordinary differential equations of second order

$$m(y(t))\ddot{y}(t) = f(t, y(t), \dot{y}(t), u(t, y(t), \dot{y}(t))) \tag{6.18}$$

where time derivatives are denoted by a dot. The *mass matrix* m represents the mass distribution within the described system, the function f comprises all (generalized) forces acting on the system. The function u is introduced to allow for a control motion, e.g. imposing a desired speed.

A constrained system can be transformed, in principle, into such a setting using Lagrange formalism. However, from a numerical point of view this is rather not desirable. A direct approach to a *differential-algebraic system*

$$\begin{aligned} m(y(t))\ddot{y}(t) &= f(t, y(t), \dot{y}(t), \lambda, u(t, y(t), \dot{y}(t))) + \nabla g\lambda & (6.19)\\ 0 &= g(t, y(t), u(t, y(t), \dot{y}(t))) & (6.20) \end{aligned}$$

leads to more efficient algorithms, [7, 8, 21, 1].

For a rigid railway wheel, for instance, we have six degrees of freedom. However, assuming that the wheel is in continuous contact with a rigid rail, the vertical shift (elevation) of the mass center can be skipped. Similarly, for a rigid wheelset both wheels of which are in contact with rails the roll angle ϕ can be evaluated for given lateral shift y and yaw angle ψ.

Figure 8: Wheelset on rails.

In both cases rather complicated geometrical calculations are required to obtain the redundant position variables from the degrees of freedom. To speed up calculations – especially for simulations in real time – one prefers to do those calculations off-line during preprocessing, [1, 3]. Of course, this works best if the bodies involved have symmetries and do not change with time. As an example, the position of the wheelset in Fig. 8 is known if the lateral shift with respect to the perfect track is known and the yaw angle is given.

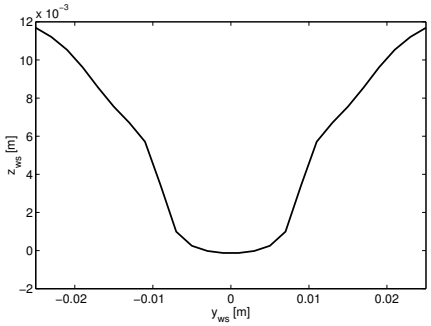

Figure 9: Elevation of wheelset.

Obviously, multiplied by load and Earth acceleration we obtain from the elevation in Fig. 9 a potential for a forces which keeps the wheelset centered. Dependence on the yaw angle (rotation around vertical axis) has been neglected here for simplicity, for more details we refer to [16] or [2, 4, 15, 20].

Position along the track and revolution angle are cyclic variables – they do not influence kinetic energy nor potential, hence they drop out of the equations for the remaining degrees of freedom. Vertical shift and roll angle are uniquely defined by lateral shift and yaw. If we denote those as y_1 and y_2, the mass matrix m becomes diagonal with entries M and I – the total mass and the moment of inertia of the wheelset. The force vector splits into one part defined by a potential obtained from the vertical shift and another one, comprising frictional force and moment, cf. [23]. An approximation to the friction forces will be described in Section 4.2.

If elasticity of the bodies in contact cannot be neglected then constraints are not adequate, in which case we have equations of motion of the form (6.18). If we allow for temporary separation of the contact partners we may have to switch between different descriptions.

There exists a number of successful simulation packages where the mentioned problems have been appropriately simplified and solved. It is worthwhile to mention that depending on the motivation some rather simple models proved most interesting, e.g. [17, 23].

For the purpose of studying wear phenomena it is obvious that we need to be able to cover relatively long time intervals. This excludes too complicated models. On the other hand, we need some minimum spatial resolution, thus a certain level of complication cannot be avoided.

6.3.2 Tangential stresses and power dissipation

We summarize here the ideas that lead to the FASTSIM algorithm, cf. [10, 18]. The normal stress is assumed to be defined by the so-called Hertz solution, [9]. Consequently, the contact patch is elliptic.

The basic quantities in this theory are the *rigid body slip* w and the *normal pressure* p_z. The latter integrates to the *normal load* N. If slip occurred everywhere, the *tangential force* would be $f_0 N$ with Coulomb's friction coefficient f_0. But due to its flexibility, the rolling body is able to minimize dissipation, it stretches in such a way that it can stick to the contact partner as long as possible. This results in much lower tangential force.

Elasticity results in a tangential displacement vector u. The main simplification of the FASTSIM approach is the postulation of a pointwise dependence

$$u = Lp\,. \tag{6.21}$$

That is, the contact partners are assumed to behave like Winkler beddings rather than elastic half-spaces or elastic bodies of the actual shape of a wheel or a rail.

Finally, the local velocity of sliding, or *local slip* is given by

$$s = w + \dot{u} = w + \frac{\partial u}{\partial x} V\,. \tag{6.22}$$

In this material time-derivative, the explicit part is dropped for the assumption of stationarity, and the y term is neglected since we consider a fast motion along the x-axis at speed V, while lateral motion has a much lower speed. Note that the notations x and y denote here locally the axes of the track coordinate system, x along the track and y in lateral direction.

Now, by taking the derivative of the norm of the tangential stress vector, we obtain by chain-rule

$$p = |\vec{p}| = \sqrt{p_x^2 + p_y^2} \quad \rightsquigarrow \quad p\frac{\partial p}{\partial x} = p_x\frac{\partial p_x}{\partial x} + p_y\frac{\partial p_y}{\partial x} \tag{6.23}$$

in the slip region. The Hertz solution to the normal problem hence leads to tangential stresses

$$p = \frac{3Nf_0}{2\pi ab}\sqrt{1 - \frac{x^2}{a^2} - \frac{y^2}{b^2}} \tag{6.24}$$

where a and b are the half axes of the contact ellipse, N is the normal load and f_0 is the friction coefficient. This allows to calculate the right-hand side of the first equation

$$p\frac{\partial p}{\partial x} = p_x\frac{\partial p_x}{\partial x} + p_y\frac{\partial p_y}{\partial x} = -\left(\frac{3Nf_0}{2\pi a^2 b}\right)^2 x\,. \tag{6.25}$$

This in turn allows to determine power dissipation, and therefore the slip

$$P_d = p_x w_x + p_y w_y + V\left(\frac{3Nf_0}{2\pi a^2 b}\right)^2 Lx \tag{6.26}$$

$$s = -\frac{P_d}{p} \qquad \vec{s} = -s\frac{\vec{p}}{p} = P_d\frac{\vec{p}}{p^2}\,. \tag{6.27}$$

Note that outside the slip region both slip and power dissipation vanish, see Fig. 11.

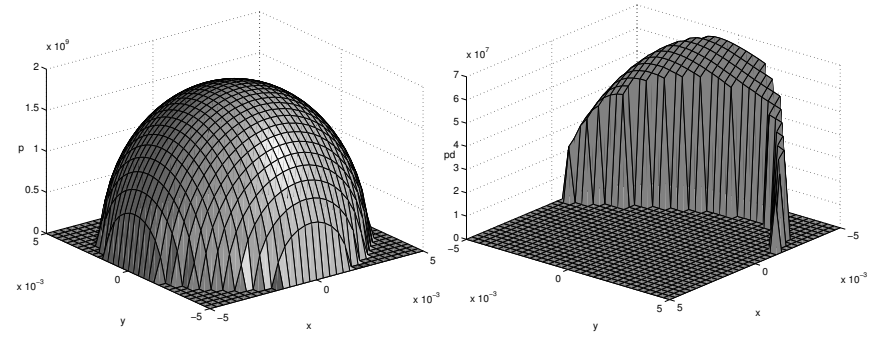

Figure 11: Hertz solution and power dissipation.

From the equation for the local slip in terms of rigid body slip and tangential strain we can obtain a reasonable approximation for strain and stress in that region. This way we obtain the friction force on the right-hand side of the MBS-equations for the vehicle, but at the same time we obtain a surface density for the dissipated power which is essential for the evaluation of wear laws.

6.3.3 Wear

Wear is a very complex process, and there is no master equation that could be applied in all possible situations. First of all, there are usually at least two bodies involved, there may be all sorts of layers between them, e.g. lubricants, dirt or worn particles of the bodies in contact. Further, the local forces and displacements at the spot where things happen are very difficult to observe and even harder to control. Usually, there is friction, and especially if dry friction is involved processes become *jerky*. In railway mechanics, the upper material layers may undergo plastification and strain hardening. There are large residual stresses. The structure of the material differs there significantly from normal. Nevertheless, for longer time intervals, wear processes can be reasonably well described in a phenomenological way. It is generally agreed that energy is needed in order to remove particles from the surfaces, cf. [5, 6]. The easiest wear laws simply assume that the mass removed from a body's surface is proportional to the energy dissipated during the wear process. Constants of proportionality can be established by grinding experi-

ments.

Some authors assume a dependence of the wear rate on the power of dissipation. For mild wear, i.e., if the energy is spread over a long time, we have a small constant, which jumps by one order of magnitude if a certain threashold is exceeded. It is assumed that under such conditions of *heavy wear* larger chunks of material are removed from the wear surfaces. However, this seems to depend on the experimental setup. Recent experiments contradict such an assumption. Furthermore, at constant power of dissipation, a time dependence of the rate of mass removal was discovered. This can be taken into account conveniently by an internal parameter responsible for the state of the surface cf. [14]. Such a parameter might reflect properties like roughness or corn size.

Locally, we obtain the surface density of dissipated power by taking the scalar product of tangential stress and relative velocity. More complicated wear laws might involve more complex dependencies of those two vector quantities, with the constraint that the response vanishes if one of the factors is zero. Most friction laws assume a linear dependence between normal load and frictional force. Also the normal load may have a more complex influence than a linear one, in particular if plastification plays a role.

Whatever wear law we assume, for our purpose it has to yield an integrable surface density of removed mass as a function of time. Divided by mass density ρ, we obtain the inwards normal speed at which the surface receeds, i.e.

$$v_n(t,\tau) = -\frac{1}{\rho}\beta P_d(t,\tau)$$

where $1/\beta$ is the energy needed to remove one unit of mass.

As input variables the multibody system coordinates and velocities together with the actual geometrical characteristics have to suffice. The proportionality law, combined with FASTSIM for the calculation of tangential stress and relative velocities, fulfills this condition and is used for the below numerical examples. Note that β is very small in SI units. That is why the evolution problem *lives* in a time scale of weeks rather than seconds.

6.4 Application

Here we put together the methods of the last two sections in order to calculate wear profiles. Given a certain geometry of a wheel profile, we are able to run a vehicle model over a track. We assume a certain period ΔT for the collection of relevant data. At $t = \Delta T$ we have a function $(t, \tau) \mapsto v_n$ assigning to each instant and place on the wear surface a wear speed. Now, we take the integral mean value of v_n over the period from $t = 0$ to $t = \Delta T$,

$$\mathcal{F}_{\Delta t}(\tau) = \frac{1}{\Delta T} \int_0^{\Delta T} v_n(t, \tau)\, dt\,.$$

We assume the existence of a limit,

$$\mathcal{F}(\tau) = \lim_{\Delta T \to \infty} F_{\Delta T}(\tau)\,.$$

We approximate this limit numerically, by increasing ΔT until $\mathcal{F}_{\Delta T}$ is practically constant within a prescribed tolerance.

Next, we perform one timestep of the manifold evolution algorithm.

This changes, of course, the wheel profile, hence all geometrical characteristics have to be adjusted. In particular, for a given lateral shift of the wheel we have now a slightly reduced elevation, a different point of contact. The curvatures at the contact point are different as well, hence the contact patch and the distribution of power dissipation over the profile will be different than in an analogous point $(y, \dot{y})$ in phase space, but at the previous stage of profile evolution.

Now, we repeat the previous steps, calculating the next $\mathcal{F}$, updating the profile and so on.

It is essential to observe that the ΔT needed for a reasonably good approximation of the limit with $\Delta T \to \infty$ (inner loop) is still by orders smaller than a time step of the evolution algorithm (outer loop).

The timestep of the outer loop is limited by stability requirements. Note that intensive wear at a certain spot rubs off material there, thus immediately reducing chances for that spot to be in contact. This leads to numerical

instabilities for too large timesteps, in particular for fine space grids – a well-known effect, e.g. in parabolic PDEs. This effect can be overcome by implicit methods, which require, however, multiple simulations of the vehicle model at the same stage of the profile evolution.

In Fig. 12 we show a worn profile, and for comparison, the initial perfect state. To make the change visible we amplify changes by a factor.

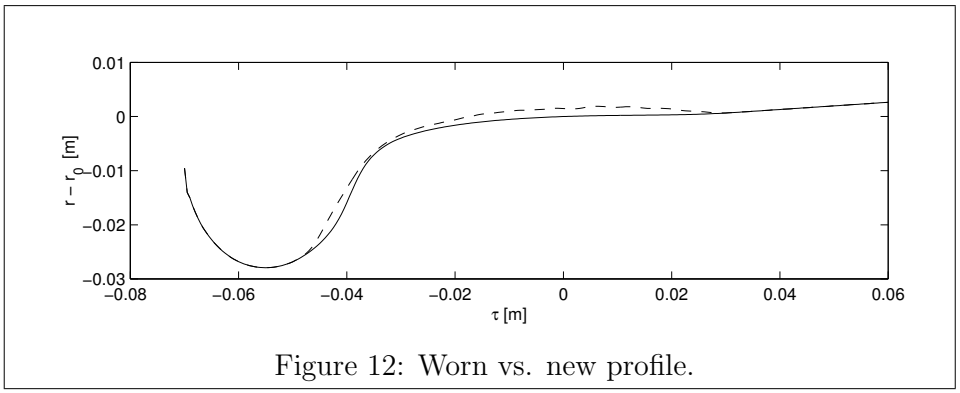

Figure 12: Worn vs. new profile.

The wear process has two negative consequences. First, obviously material is lost, hence the wheel tyre is becoming thinner and thinner, until the wheel must be exchanged. Second, the uniform wear process may become unstable, and certain spatial patterns may evolve. Typical of highspeed trains is so-called *polygonalisation*. Instead of a constant profile in angular direction, one observes a series of minima and maxima along the circumference of the wheel. This process is related to accelerations in vertical direction. Polygonalisation results in unpleasant sound (grumbling of ICE trains) and in considerably larger speed of wear. Without going into details, we present here in Fig. 13 the result of a simulation.

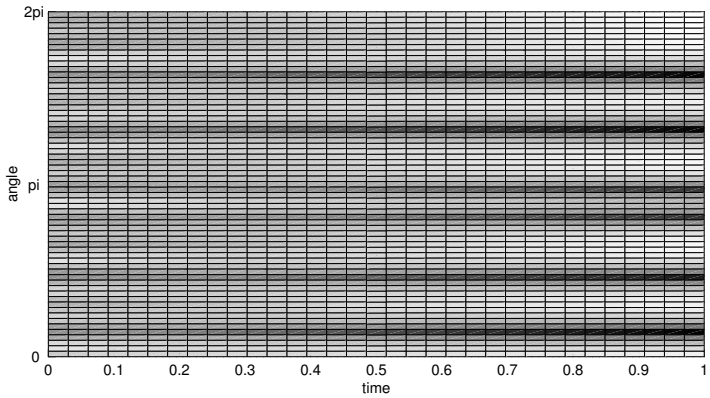

Figure 13: Polygonalisation.

The time t runs from zero to one – the lifetime of the wheel. On the vertical axis we see the angular surface coordinate τ. Initially, the radius (integral mean over lateral coordinate) is nearly constant. Later a number of humps evolves in a self-excited manner. The change of radius is represented by graylevel.

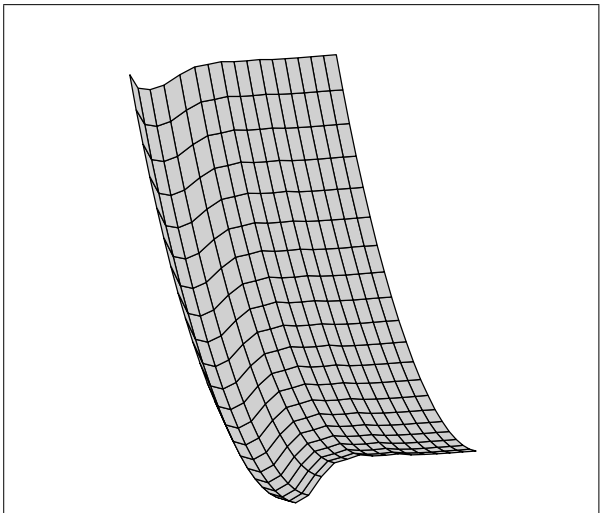

Figure 14: Segment of a worn wheel surface.

Fig. 14 shows a segment of a out-of the-round worn wheel surface, i.e. with changes both in profile and along the circumference.

6.5 Conclusions

The study of wear processes is still a wide field. One needs to resolve two extremely different time scales. The dynamical behavior of vehicles decides about the speed of wear, and it needs a resolution much smaller than one second. The evolution of a wheel's of rail head's shape takes weeks or months to show visible effects. Thus the problem fits into the framework of evolving manifolds, where the speed law has to be evaluated by numerical simulations of dynamical systems. However, reasonable approximations for the contact forces still beat a brute force approach.

We succeeded with the calculation of curvature driven evolution even for fairly *wild* domains as in Fig. 3 or 6. In particular, we can preserve sharp edges for hyperbolic-like cases. In application to rail–wheel problems we obtain realistic wear patterns.

Bibliography

[1] M. Arnold, K. Frischmuth. Solving problems with unilateral constraints by DAE methods. Mathematics and Computers in Simulation 47:47-67, 1998.

[2] K. Frischmuth, M. Arnold, M. Hänler, H. Netter. Differentialgleichungen und singuläre Mannigfaltigkeiten in der dynamischen Simulation von Rad-Schiene-Systemen, in: Hoffmann, Jäger, Lohmann, Schunck (Eds.), Mathematik – Schlüsseltechnologie für die Zukunft, Proceedings des BMBF-Statusseminars München 1995. Springer-Verlag Berlin/Heidelberg, 1996.

[3] M. Arnold, H. Netter. Approximation of contact geometry in the dynamical simulation of wheel-rail systems. Mathematical and Computer Modelling of Dynamical Systems 4:162-184, 1998.

[4] R. Bogacz, S. Dżula. Dynamics and stability of a wheelset in rolling contact motion on rails, in: Proc. of ITTG International Symposium on the Technological Innovation in Guided Transports, pp. 871–883. Lille, 1993.

[5] E. Brommundt. A simple mechanism for the polygonalization of railway wheels by wear, Mechanics Research Communications Basic and Applied, 1996.

[6] A. Chudzikiewicz. Zużycie kół kolejowych, in: Proceedings of the 7th Conference on Computer Simulation in Research and Development. Kościelisko, September 14–26, 2000.

[7] C.W. Gear, G.K. Gupta, and B. Leimkuhler. Automatic integration of Euler–Lagrange equations with constraints. J. Comp. Appl. Math., 12&13:77–90, 1985.

[8] E. Hairer and G. Wanner. Solving Ordinary Differential Equations. II. Stiff and Differential-Algebraic Problems. Springer-Verlag, Berlin Heidelberg New York, 1991.

[9] H. Hertz. Über die Berührung fester elastischer Körper. J. reine und angewandte Mathematik 92, 1882.

[10] J. J. Kalker. Three-Dimensional Elastic Bodies in Rolling Contact. Vol. 2 of Solid Mechanics and its Applications. Kluwer Academic Publisher, Dordrecht, 1990.

[11] K. Frischmuth. On the numerical solution of rail-wheel contact problems. J. Theoretical and Applied Mechanics, 34, 1, 7–15, 1996

[12] K. Frischmuth, Rail-wheel contact, dynamical simulation and damage, in: W. Kosiński, R. de Boer, D. Gross (Eds.) Problems of Environmental and Damage Mechanics, IPPT PAN, Warszawa, pp. 149–156, 1997.

[13] K. Frischmuth, D. Langemann. Numerical analysis of long-term wear models. Machine Dynamics Problems, 20, pp. 113–122, 1998.

[14] K. Frischmuth. Wear models with internal state parameters. Machine Dynamics Problems, 24, No. 1, pp. 79–86, 2000.

[15] K. Frischmuth. On the temporal evolution of wear profiles, in: Z. Strzyżakowski and P. Lesiak (Eds.) Proceedings of the 4^{th} TransComp Conference. Zakopane, December 6–8, 2000.

[16] K. Frischmuth. Contact, motion and wear in railway mechanics. Submitted to Journal of Theoretical and Applied Mechanics, 2001.

[17] Ch. Kaas-Petersen. Chaos in a Railway Bogie. Acta Mechanica **61** pp. 89–107, 1986.

[18] W. Kik, J. Piotrowski. A fast, approximate method to calculate normal load at contact between wheel and rail and creep forces during rolling, in: I. Zobory (Ed.) Proc. of the 2nd MiniConference on Contact Mechanics and Wear of Rail/Wheel Systems, pp. 52–61. TU Budapest, 1996.

[19] D. Langemann. Numerische Analyse abrasiv verschleißender mechanischer Systeme. Fortschritt-Berichte 12.392, VDI-Verlag Düsseldorf, 1999.

[20] P. Meinke. Über das Entgleisen von Radsätzen, in: K. Frischmuth (Ed.), Proceedings of the 7th Workshop on Dynamics of Rail/Wheel dynamics. Rostock, June 13–14, 2000.

[21] B. Simeon, C. Führer, and P. Rentrop. Differential-algebraic equations in vehicle system dynamics. Surveys on Mathematics for Industry, 1:1–37, 1991.

[22] J. A. Sethian. Level set methods. Cambridge University Press, Cambridge, 1996.

[23] H. True. Dynamics of a rolling wheelset. Applied Mechanics Reviews, vol. 46, Nr. 7, 1993.